J Mater Sci (2010) 45:633–640
DOI 10.1007/s10853-009-3977-7

The effect of multi-walled carbon nanotubes addition on the thermo-oxidative decomposition and flammability of PP/MWCNT nanocomposites

Azat D. Rakhimkulov · S. M. Lomakin · I. L. Dubnikova · A. N. Shchegolikhin · E. Ya Davidov · R. Kozlowski

Received: 17 April 2009 / Accepted: 12 October 2009 / Published online: 24 October 2009

Abstract Studies of thermo-oxidative and fire-resistant properties of the polypropylene/multi-walled carbon nanotube composites (PP/MWCNT) prepared by melt intercalation are discussed. The effective kinetic parameters of the PP/MWCNT thermo-oxidative decomposition were computed according to the model-based kinetic analysis. The thermo-oxidative decomposition behavior of PP/MWCNT and stabilizing effect caused by addition of MWCNT has been investigated by means of TGA and EPR spectroscopy. Comparative analysis of the flammability characteristics for PP-clay/MWCNT nanocomposites was provided in order to emphasize the specific behavior of the nanocomposites.

Introduction

At present time the great attention is given to the study of properties of polymeric nanocomposites produced on the basis of well-known thermoplastics (PP, PE, PS, PMMA, polycarbonates, polyamides) and carbon nanotubes (CNs). CNs are considered to have the wide set of important properties like thermo-oxidative stability, reduced flammability, electroconductivity, etc. [1–7]. Thermoplastic polymer nanocomposites are generally produced with the use of melting technique [1–12].

Development of synthetic methods and the study of thermal and thermo-oxidative characteristics of polypropylene/multi-walled carbon nanotube (PP/MWCNT) nanocomposites were taken as an objective in this paper.

A number of papers pointed at synthesis and research of thermo-oxidative properties of nanocomposites (atactic polypropylene (aPP)/MWCNT) were reported [10–12]. It is remarkable that PP/MWCNT composites with minor level of nanocarbon content (1–5 wt%) were determined to obtain an increase in thermal and thermo-oxidative stability in the majority of these publications.

Thermal stability of aPP and aPP/MWCNT nanocomposites with the various concentrations of MWCNT in nitrogen atmosphere was studied in the paper [10]. It was shown that thermal decomposition processes are similar for aPP and aPP/MWCNT nanocomposites and initial decomposition temperatures are the same. However, the maximum mass loss rate temperature of PP/MWCNT nanocomposites with 1 and 5 wt% of MWCNT raised by 40–70 °C as compared with pristine aPP.

Kashiwagi et al. [11, 12] published the results of study of thermal, thermo-oxidative, and flammability properties of PP/MWCNT nanocomposites. A significant decrease of maximum heat release rate was detected during the flammability research with the use of cone calorimeter. A formation of char network structure during the process was considered to be the main reason of flammability decrease. The carbonization influence upon flammability of polymeric nanocomposites was widely presented in literature [10–13]. Notably, Kashiwagi et al. [11, 12] were the first to hypothesize that abnormal dependence of maximum heat release rate upon MWCNT concentration is closely related with thermal conductivity growth of PP/MWCNT

A. D. Rakhimkulov (✉) · S. M. Lomakin · A. N. Shchegolikhin · E. Y. Davidov
NM Emanuel Institute of Biochemical Physics of Russian Academy of Sciences, Kosygin 4, 119934 Moscow, Russia
e-mail: azat.rakhimkulov@mail.ru

I. L. Dubnikova
NN Semenov Institute of Chemical Physics of Russian Academy of Sciences, Kosygin 4, 119991 Moscow, Russia

R. Kozlowski
Institute of Natural Fibres, ul. Wojska Polskiego 71 b, Poznan, Poland

nanocomposites during high-temperature pyrolysis and flammability tests.

Experimental

Materials

Isotactic polypropylene (melting flow index = 0.7 g/10 min) was used as a polymer matrix in this paper. MWCNT (purchased from Shenzhen Nanotechnologies Co. Ltd.) were used as carbon-containing nanofillers. This product contains low amount of amorphous carbon (less than 0.3 wt%). Size characteristics for MWCNT used in this paper are given in Table 1. Sizes and structure of initial MWCNT were additionally estimated by SEM (Fig. 1).

Nanocomposite processing

Compositions were prepared by blending carbon nanotubes with melted polymer in a laboratory mixer Brabender at 190 °C. TOPANOL® (1,1,3-tris(2-methyl-4-hydroxy-5-*t*-butylphenyl)butane) and DLTP (dilaurylthiodipropionate) were added in the amount of 0.3 and 0.5 wt% as antioxidants to prevent thermo-oxidative decomposition during polymer processing.

Table 1 Properties of MWCNT

Designation	*D* (nm)	*L* (μm)	Density (g/cm^3)	Specific surface area (m^2/g)
MWCNT	40–60	5–15	2	40–300

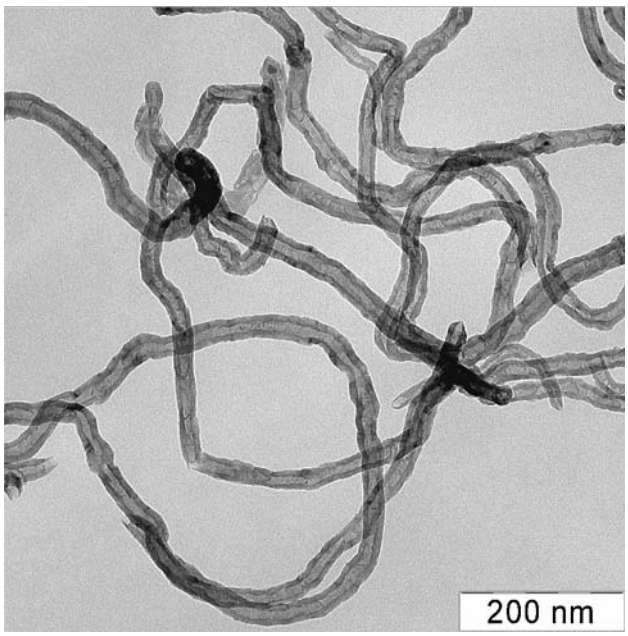

Fig. 1 SEM images of original MWCNTs

A number of different covalent and non-covalent nanotube modifications (organofillization) were reported to be used to achieve greater structure similarity and therefore greater nanotube distribution in a polymer matrix [14–23]. In order to functionalize MWCNT we used preliminary ozone treatment of MWCNT followed by ammonolysis of epoxy groups on the MWCNT surface. The selective ozonization of MWCNT was carried out with ozone–oxygen mixture (ozone concentration was 2.3×10^{-4} mol/L) in a bubble reactor. Then the ammonolysis of oxidized MWCNT has been carried out by *tert*-butylamine in the ultrasonic bath (35 kHz) at 50 °C for 120 min with following evaporation of *tert*-butylamine excess. IR transmission spectra of tablet specimens of MWCNTs in KBr matrix was analyzed by using Perkin-Elmer 1725X FTIR spectrometer and the presence of the alkylamine groups at the MWCNT surface was confirmed by the appearance of the characteristic band ~ 1210 cm^{-1} corresponding to the valency vibration of the bond C–N.

The nanocomposites of PP/MAPP/MMT used for comparison were obtained as follows. PP (MFI = 0.7) and maleic anhydride-modified oligomer (MAPP—Licomont AR 504 by Clariant co.) with *M*n ~ 2900; MA content ~ 4 wt% were blended/mixed using a laboratory Brabender mixing chamber for 2 min at the first stage. The concentration of MAPP was 20% by weight of original PP. Then the organoclay (Cloisite 20A by Southern Clay Co.) was added to the PP–MAPP melt at the temperature of 190 °C. 10 min mixing time was used in all the experiments [24].

Investigation techniques

Scanning electron microscopy (SEM) The degree of MWCNT distribution in polymer matrix was analyzed with scanning electron microscope JSM-35. Low-temperature chips derived from film-type samples were used for this analysis.

Transmission electron microscopy (TEM) The degree of nanotube dispersion in polymer matrix was studied with transmission electron microscopy (LEO912 AB OMEGA, Germany). Microscopic sections with 70–100 nm width prepared with ultramicrotome "Reichert–Jung Ultracut" with diamond cutter at −80 °C. Microscopic analysis was made with accelerating potential of about 100 kV without chemical sample staining.

Thermogravimetric analysis (TGA) A NETZSCH TG 209 F1 Iris thermomicrobalance has been employed for TGA measurements in oxidizing (oxygen) atmosphere. The measurements were carried out at a heating rate of 20 K/min.

Flammability characteristics (cone calorimeter) were performed according to the standard procedures ASME E1354/ISO 5660 using ATLAS CONE2 cone-calorimeter. An external radiant heat flux of 35 kW/m^2 was applied. All of the samples having a standard surface area of 70 × 70 mm, thickness of 3 mm, and identical masses of 13.0 ± 0.2 g were measured in the horizontal position and wrapped with thin aluminum foil except for the irradiated sample surface.

Heat capacity and heat conductivity were determined with the use of NETZSCH 457 *MicroFlash.*

The electron paramagnetic resonance spectroscopy (EPR) measurements were performed in air with the PP/MWCNT (10 wt%) samples using a Mini-EPR SPIn Co. Ltd spectrometer with 100 kHz field modulation. The *g* factor and EPR intensity (X-band) were measured with respect to a standard calibrating sample of Mn^{2+} and ultramarine.

Results and discussion

Nanocomposite structure

Dispersion analysis of MWCNT in nanocomposites. PP/MWCNT nanocomposites with original and modified MWCNT were produced. Filler concentration varied from 1–5 wt% (0.5–2.5 vol%, correspondingly). Distribution pattern for composites with modified and non-modified nanotubes was studied with TEM methods (Fig. 2). According to TEM images the addition of 1% by weight leads to sufficiently uniform distribution. However, agglomeration of nanotubes was detected for more concentrated nanocomposites.

Figure 2 shows TEM images for PP nanocomposites with 5 wt% (a) modified and (b) non-modified MWCNTs. According to Fig. 2 it could be stated that modified and non-modified nanotubes used during melting process are present as individual particles in nanocomposite in most cases. However, preliminary modification does not lead to any significant distribution advantage. Thus, in this study we used non-modified MWCNTs mostly.

In further comparison we used the data for PP/MMT nanocomposites obtained earlier [24]. On the basis of results obtained using XRD, TEM, and AFM techniques, authors characterize the structure of the PP/MMT nanocomposite obtained by melt intercalation as a structure of a mixed hybrid type in which polymer–silicate intercalation nanoclusters coexist with delaminated-filling regions [24]. Information on the structure of the PP/MPP/MMT nanocomposite was obtained with the use of TEM (Fig. 3). TEM photographs at various magnifications clearly show regions of intercalated stacks (tactoids) containing ten or more laminar silicate layers (*B*), as well as zones with the delaminated silicate structure in which individual monolayers are present (*A*).

The number of individual monolayers was counted and the statistical distribution in a certain selected region of the microphotograph of 500 × 500 nm in size was estimated with the use of the Noesys VISILOG 6.3 software program [24]. As a distribution criterion, authors took the magnitude of the ratio of geometric dimensions of the monolayer length *l* to the mean monolayer thickness *d* (1.5 ± 0.5 nm) [24]. On the basis of the obtained data, it was concluded that the majority of monolayers have the size ratio of $l{:}d \sim 75$, while the length of silicate layers in intercalated nanoclusters ranges within 100–300 nm [24].

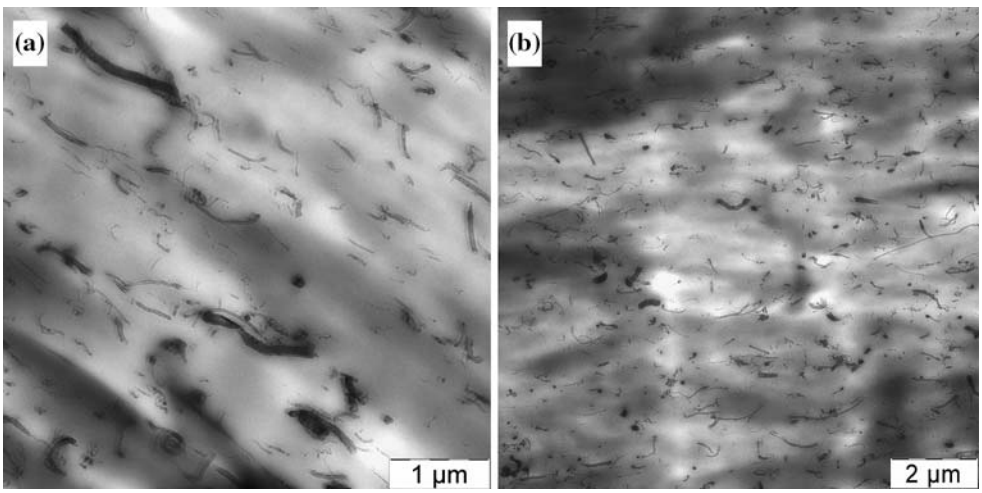

Fig. 2 TEM images of PP/MWCNT nanocomposites showing dispersion of MWCNT in a polymer matrix: **a** PP/MWCNT(non-modified), **b** PP/MWCNT(modified)

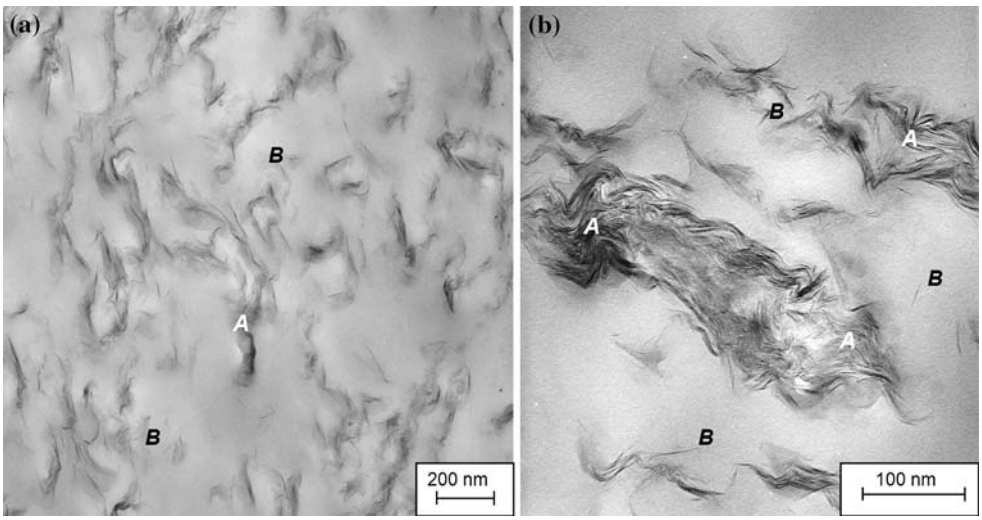

Fig. 3 TEM photograph of the PP/MPP/MMT nanocomposite: (*A*) zones with delaminated silicate structure and (*B*) intercalation region [24]

On the basis of the above consideration, we may characterize the structure of the PP/MPP/MMT nanocomposite obtained by melt intercalation as a structure of a mixed hybrid type in which polymer–silicate intercalation nanoclusters coexist with delaminated-filling regions.

Thermo-oxidative decomposition of PP/MWCNT nanocomposites

The diverse behavior of PP and PP/MWCNT nanocomposites with 1, 3, and 5 wt% of MWCNT (Fig. 4) shows that the influence of MWCNTs on the thermo-oxidation process resulted in higher thermo-oxidative stability of PP/MWCNT nanocomposites. It is possible to see a regular increase in the temperature values of the maximum mass loss rates (up to 60 °C) for the PP/MWCNT as compared to pristine PP (Fig. 4).

Detailed analysis of TGA graphs (Fig. 4) allows claiming that thermo-oxidative stability increase is achieved even by addition of 1 wt% of MWCNT to PP, while further addition does not lead to such fundamental growth. In addition, Fig. 5 shows the comparative results for onset decomposition temperatures ($T_{on.}$) and the maximum mass loss temperatures (T_{max}) of PP/MWCNT nanocomposites in air atmosphere with the different types and concentrations of MWCNT. One can see non-linear relation of ($T_{on.}$) and (T_{max}) versus MWCNT concentration in the PP compositions (Fig. 5).

Additional TGA tests of PP and 3 and 5 wt% PP/MWCNT nanocomposites in argon atmosphere were performed (Fig. 6). A small difference in thermal stability was detected—4° and 10° increase for nanocomposites with 3 and 5 wt% of MWCNT, correspondingly, compared

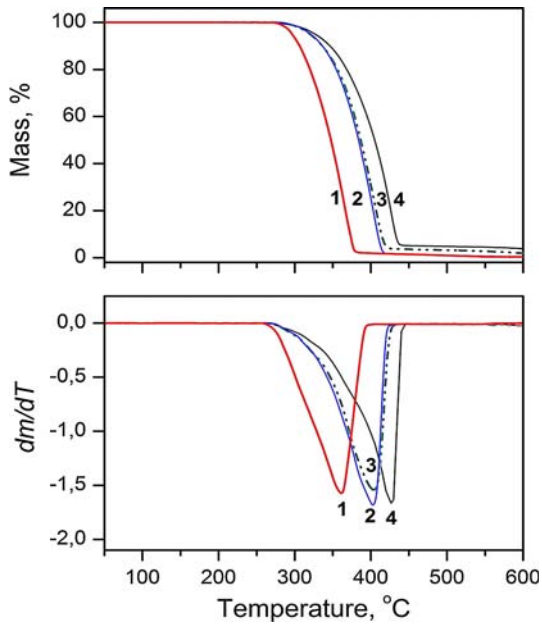

Fig. 4 TG and DTG curves for PP (*1*) and PP/MWCNT nanocomposites with 1 (*2*), 3 (*3*), and 5 wt% (*4*) filler loadings in air atmosphere

to pristine PP. The mass residues after performed TGA in argon atmosphere shows values close to initial mass of added MWCNT—3.4 and 6.1 wt% residues for 3 and 5 wt% of MWCNT nanocomposites.

At the present time the nature of thermo-oxidative stability effect caused by MWCNT addition to polymers is an object of comprehensive study. Most likely, MWCNTs could be considered as high-temperature stabilizers (antioxidants) in reactions of thermo-oxidative decomposition by analogy with fullerenes [25]. Stabilizing effect caused by addition of MWCNT was previously detected for

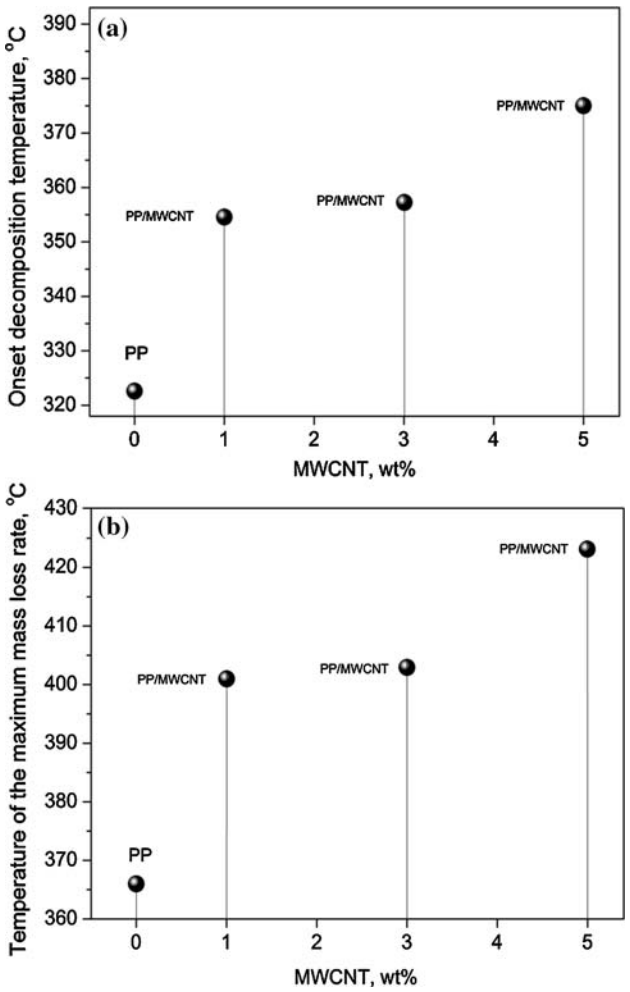

Fig. 5 Comparative diagrams showing the onset decomposition temperatures (**a**) and the maximum mass loss temperatures (**b**) for PP and PP/MWCNT nanocomposites with the different types and concentrations of MWCNT

PP/MWCNT nanocomposites [8]: the temperature of the maximum mass loss rates of PP/MWCNT (9 wt%) was increased by 50 °C as compared with pristine PP.

Results achieved in this study confirm the previous findings of the inhibiting effect of MWCNT upon the PP/MWCNT nanocomposite thermo-oxidative decomposition. Obviously, the complex nature of this effect is closely related to radical-acceptor properties of MWCNT resulting in chain termination reactions of alkyl/alkoxyl radical, which lead to cross-linking and carbonization process in PP/MWCNT nanocomposites.

Kinetic analysis of thermo-oxidative decomposition of PP/MWCNT

Kinetic studies of material decomposition have long history, and there exists a long list of data analysis techniques

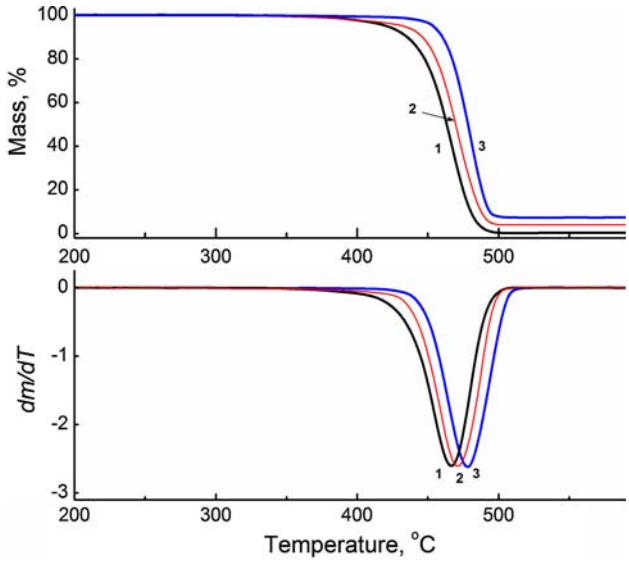

Fig. 6 TG and DTG curves for PP (*1*) and PP/MWCNT nanocomposites with 3 (*2*) and 5 (*3*) wt% filler loadings in argon atmosphere

employed for the purpose. Often, TGA is the method of choice for acquiring experimental data for subsequent kinetic calculations, and namely this technique was employed here. It is commonly accepted that the decomposition of materials follows the base equation (1) [26]

$$dc/dt = -F(t, T, c, p) \quad (1)$$

where: t—time, T—temperature, c_0—initial concentration of the reactant, and p—concentration of the final product. The right hand part of the equation $F(t, T, c, p)$ can be represented by the two separable functions, $k(T)$ and $f(c, p)$:

$$F(t, T, c, p) = k[T(t) \cdot f(c, p)] \quad (2)$$

Arrhenius equation (4) will be assumed to be valid for the following:

$$k(T) = A \cdot \exp(-E/RT) \quad (3)$$

Therefore,

$$dc/dt = -A \cdot \exp(-E/RT) \cdot f(c, p) \quad (4)$$

All feasible reactions can be subdivided onto classic homogeneous reactions and typical solid-state reactions, which are listed in Table 2. The analytical output must provide good fit to measurements with different temperature profiles by means of a common kinetic model.

Thermogravimetric analysis of PP and PP nanocomposite decomposition was carried out in dynamic conditions at the rates of 2.5, 5, and 10 K/min on air.

Model-free estimation of activation energy using Friedman approach [27] was taken to get preliminary model analysis for thermo-oxidative decomposition and selection of initial conditions. According to this evaluation, a two-step process ($A \rightarrow X_1 \rightarrow B \rightarrow X_2 \rightarrow C$) was chosen for PP

Table 2 Considered reaction models $dc/dt = -A \cdot \exp(-E/RT)f(c, p)$

Reaction models	$f(c, p)$
First order (F_1)	c
Second order (F_2)	c^2
n-Order (F_n)	c^n
Two-dimensional phase boundary (R_2)	$2 \cdot c^{1/2}$
Three-dimensional phase boundary (R_3)	$3 \cdot c^{2/3}$
One-dimensional diffusion (D_1)	$0.5/(1 - c)$
Two-dimensional diffusion (D_2)	$-1/\ln(c)$
Three-dimensional diffusion, Jander's type (D_3)	$1.5c^{1/3}(c^{-1/3} - 1)$
Three-dimensional diffusion, Ginstling-Brounstein (D_4)	$1.5/(c^{-1/3} - 1)$
One-dimensional diffusion (Fick law) (D_{1F})	–
Three-dimensional diffusion (Fick law) (D_{3F})	–
Prout-Tompkins equation (B_1)	$c \cdot p$
Expanded Prout-Tompkins equation (B_{na})	$c^n \cdot p^a$
First order reaction with autocatalysis by X (C_{1-X})	$c \cdot (1 + K_{cat} X)$
n-order reaction with autocatalysis by X (C_{n-X})	$c^n \cdot (1 + K_{cat} X)$
Two-dimensional nucleation, Avrami-Erofeev equation (A_2)	$2 \cdot c \cdot (-\ln(c))^{1/2}$
Three-dimensional nucleation, Avrami-Erofeev equation (A_3)	$3 \cdot c \cdot (-\ln(c))^{2/3}$
n-dimensional nucleation, Avrami-Erofeev equation (A_n)	$n \cdot c \cdot (-\ln(c))^{(n-1)/n}$

decomposition. Taking into account the carbonization stage the more complex three-step process ($A \rightarrow X_1 \rightarrow B \rightarrow X_2 \rightarrow C \rightarrow X_3 \rightarrow D$) was selected for PP/MWC NT decomposition [26, 28].

According to the results of non-linear regression and taking the set of reaction models into consideration we computed the values of effective kinetic parameters, which represent the best approximation of experimental TGA graphs (Fig. 7; Table 3).

Two-step PP thermo-oxidative decomposition in dynamic heating conditions was confirmed by obtained data [24]. At the first stage the values of activation energy and pre-exponential factor are 110.25 kJ/mol and $10^{9.5}$ s^{-1}, correspondingly, while the reaction order is close to 2 (1.89). The values of activation energy and pre-exponential factor are larger on the second stage ($E_2 = 150.65$ kJ/mol, $A_2 = 10^{15.3}$ s^{-1}) with effective reaction order of $n_2 = 1.50$.

The preferred model for PP/MWCNT thermo-oxidative decomposition and with respect to statistical analysis of kinetic parameters is composed of 3 consecutive reactions $F_n \rightarrow D_1 \rightarrow F_n$, where D_1—one-dimensional diffusion and F_n—n-order reaction (Fig. 7b; Table 3b). In this case the first-step activation energy is equal to 105.1 kJ/mol, reaction order is close to 1 ($n_1 = 0.91$). On the second step, which is described as one-dimensional diffusion, the value of activation energy is equal 120.4 kJ/mol, while the value is almost twice large for the third step ($E_3 = 229.5$ kJ/mol) with effective reaction order of $n_3 = 0.5$ (Table 3b).

Comparison of thermo-oxidative decomposition parameters for PP/MWCNT with layered silicate PP/MPP/MMT showed that the values of activation energy of the second

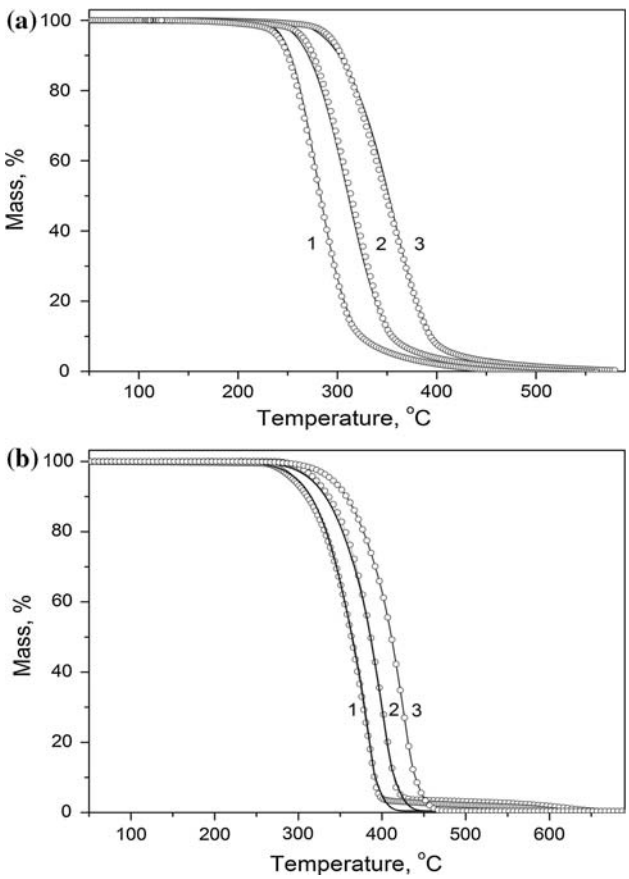

Fig. 7 Non-linear kinetic modeling of **a** PP and **b** PP/MWCNT thermo-oxidative decomposition in air. Comparison between experimental TG data (*dots*) and the model results (*firm lines*) at several heating rates: (*1*) 2.5, (*2*) 5, (*3*) 10 K/min

Table 3 Kinetic parameters for thermo-oxidative decomposition of PP ($F_n \rightarrow F_n$) and PP/MWCNT nanocomposite ($F_n \rightarrow D_1 \rightarrow F_n$)

Reaction model	Kinetic parameters	Values	Correlation coefficient
PP nanocomposite			
$F_n \rightarrow F_n$	log A_1, s^{-1}	9.53	0.9996
	E_1, kJ/mol	110.25	
	n_1	1.89	
	log A_2, s^{-1}	15.25	
	E_2, kJ/mol	150.65	
	n_2	1.50	
PP/MWCNT nanocomposite			
$F_n \rightarrow D_1 \rightarrow F_n$	log A_1, s^{-1}	6.3	0.9996
	E_1, kJ/mol	105.1	
	n_1	0.91	
	log A_2, s^{-1}	7.4	
	E_2, kJ/mol	120.4	
	log A_3, s^{-1}	16.7	
	E_3, kJ/mol	229.5	
	n_3	0.5	

TGA analysis was performed in air flow with the use of multiple non-linear regression analysis for model processes

and the third stages are higher for PP/MWCNT: $E_2 = 120.4$ kJ/mol and $E_3 = 229.5$ kJ/mol for PP/MWCNT; $E_2 = 100.0$ kJ/mol and $E_3 = 199.8$ kJ/mol for PP/MPP/MMT, correspondingly [24].

This data may testify to more intensive oxidative carbonization in case of PP/MWCNT than in case of PP/MPP/MMT.

In the present study EPR research was performed to follow formation of paramagnetic centers relating to carbonaceous sites and responsible for carbonization process, upon isothermal heating of PP/MCWNT (10 wt%) in air at 350 °C.

Figure 8a shows EPR spectrum of the stable paramagnetic centers formed in the samples of PP/MCWNT (10 wt%) heating in air at 350 °C. When heated in air

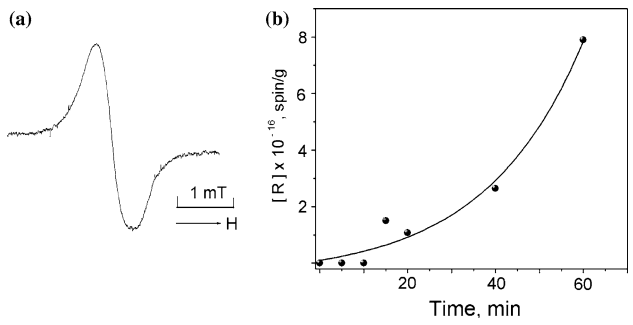

Fig. 8 EPR spectrum of the stable paramagnetic centers formed in the samples of PP/MCWNT (10 wt%) heating in air at 350 °C (**a**), kinetic dependence of stable radicals generation from PP/MCWNT (10 wt%) under isothermal heating at 350 °C in air (**b**)

PP/MCWNT specimen was placed into an EPR sample tube, a narrow singlet signal with a line width of $\Delta H_{1/2} = 0.69$ mT and a g value of 2.003 was detected due to the stable radicals generation, analogous to those previously registered during polymers carbonization process [29]. No EPR signal similar to that of PP/MCWNT samples were observed in the samples of pristine PP and MCWNT samples heated at 350 °C in air. It should be noted that although iron impurity from MWCNT has been mentioned in other studies on pyrolysis of polymer nanocomposites as the radical traps [11, 30], the EPR analyses in the current study showed the presence of paramagnetic centers relating to carbonaceous sites only.

As it is seen from Fig. 8b, the formation of stabilized radicals occurs with pronounced induction period which is related to antioxidant properties of MWCNT. Such a type of kinetic dependence is coincided with an oxygen uptake kinetics observed during inhibited polyolefines thermal oxidation. Moreover, no EPR signals were observed in the samples of the PP/MCWNT samples heated at 350 °C in inert Ar.

Additional isothermal decomposition tests of the PP/MCWNT (10 wt%) and pristine PP in air at the temperature of 400 °C lasting for 30 min were performed. The obtained data showed complete degradation/volatilization with no mass residue for pristine PP. However, the residue (18 wt%) was detected for PP/MCWNT (10 wt%) nanocomposite.

Flammability of PP/MWCNT nanocomposites

Figure 9 depicts the plots of the heat release rate (RHR), as basic flammability characteristic, versus time for PP, as well as for the PP/MWCNT nanocomposites.

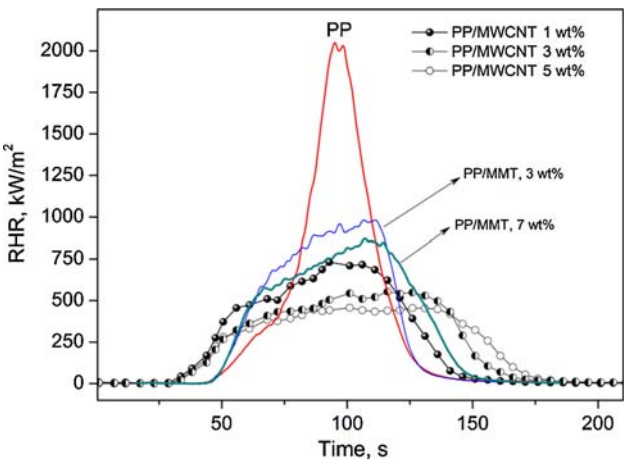

Fig. 9 Rate of heat release versus time for PP, PP/MWCNT, and PP/MPP/MMT nanocomposites obtained by cone calorimeter at the incident heat flux of 35 kW m^{-2}

From Fig. 9, it could be seen that the maximum heat release rate for pristine PP is 2076 kW/m^2, whereas that for the PP/MWCNT nanocomposites (1 wt%), PP/MCWNT (3 wt%), and the PP/MCWNT (5 wt%) RHR values are 729, 552.8, and 455.8 kW/m^2, respectively; thus, the peak heat release rate decreases by 65, 73, and 78%.

The observed flame retardancy effect is associated with shielding effect, by analogy with layered silicates [31, 32]. In early paper [24] we have found that additions of 3 and 7 wt% of layered silicate (Cloisite 20A) to the PP compositions lead to RHR decrease by 51 and 57% as compared with pristine PP (Fig. 9).

The mass of fire residues for PP/MWCNT 1, 3, and 5 wt% nanocomposites are 1.2, 2.3, and 2.6%, correspondingly. The similar data for PP/MPP/MMT 3 and 7 wt% nanocomposites are 2.5 and 6.1%.

It was proposed previously that the observed improvement in flammability properties is mainly based on the processes in the condensed phase where the nanotube network layer acts as a thermal shield to reduce the exposure of the polymer in the nanocomposite to a fire [11]. The flocculated network layer (MWCNT) is most effective for reducing flammability if it uniformly covers the entire sample surface. This is achieved by forming the networked floccule structure, which has physical integrity without breaking during burning.

A protective layer was also observed with PP/MPP/MMT nanocomposites, but the layer was less uniform and weak as compared with PP/MWCNT due to original hybrid (intercalated/delaminated) type structure of the PP/MPP/MMT nanocomposite. That is why the protective layer of PP/MPP/MMT nanocomposite is less effective as a barrier for degradation products of PP.

Thus, multi-walled carbon nanotubes are considered to be more effective filling agents than layered silicates in the terms of improvement of thermo-oxidative properties and fire behavior of PP matrix.

References

1. Shaffer MSP, Windle AH (1999) Adv Mater 11:937
2. Qian D, Dickey EC, Andrews R, Rantell T (2000) Appl Phys Lett 76:2868
3. Jin Z, Pramoda KP, Xu G, Goh SH (2001) Chem Phys Lett 337:43
4. Thostenson ET, Chou TW (2002) J Phys D Appl Phys 35:L77
5. Bin Y, Kitanaka M, Zhu D, Matsuo M (2003) Macromolecules 36:6213
6. Potschke P, Dudkin SM, Alig I (2003) Polymer 44:5023
7. Safadi B, Andrews R, Grulke EA (2002) J Appl Polym Sci 84:2660
8. Watts PCP, Fearon PK, Hsu WK, Billingham NC, Kroto HW, Walton DRM (2003) J Mater Chem 13:491
9. Watts PCP, Hsu WK, Randall DP, Kroto HW, Walton DRM (2002) Phys Chem Chem Phys 4:5655
10. Jun Y, Yuhan L, Jinfeng W (2005) J Appl Polym Sci 98(3):1087
11. Kashiwagi T, Grulke E, Hilding J, Groth K, Harris RH, Butler K, Shields JR, Kharchenko S, Douglas J (2004) Polymer 45:4227–4239
12. Kashiwagi T, Grulke E, Hilding J, Harris RH Jr, Awad WH, Douglas J (2002) Macromol Rapid Commun 23:761
13. Lomakin SM, Novokshonova LA, Brevnov PN, Shchegolikhin AN (2008) J Mater Sci 43(4):1340. doi:10.1007/s10853-007-2295-1
14. Chen J, Hamon MA, Hu H, Chen Y, Rao AM, Eklund PC, Haddon RC (1998) Science 282:95
15. Stevens JL, Huang AY, Peng H, Chiang IW, Khabashesku VN, Margrave JL (2003) Nano Lett 3:331
16. Eitan A, Jiang K, Dukes D, Andrews R, Schadler LS (2003) Chem Mater 15:3198
17. Hu H, Ni Y, Montana V, Haddon RC, Parpura V (2004) Nano Lett 4:507
18. Kong H, Gao C, Yan D (2004) J Am Chem Soc 126:412
19. Holzinger M, Vostrowsky O, Hirsch A, Hennrich F, Kappes M, Weiss R, Jellen F (2001) Angew Chem Int Ed 40:4002
20. Holzinger M, Abraham J, Whelan P, Graupner R, Ley L, Hennrich F, Kappes M, Hirsch A (2003) J Am Chem Soc 125:8566
21. Yao Z, Braidy N, Botton GA, Adronov A (2003) J. Am.Chem. Soc. 125:16015
22. Ying Y, Saini RK, Liang F, Sadana AK, Billups WE (2003) Org Lett. 5:1471
23. Alvaro M, Atienzar P, de la Cruz P, Delgado JL, Garcia H, Langa F (2004) J Phys Chem B 108:12691
24. Lomakin SM, Dubnikova IL, Berezina SM, Zaikov GE (2006) Polym Sci Ser A 48(1):72
25. Krusic J, Wasserman E, Keizer PN, Morton JR, Preston KF (1991) Science 254:1183
26. Opfermann J (2000) J Therm Anal Calorim 60(3):641
27. Friedman HL (1965) J Polym Sci 6:175
28. Opfermann J, Kaisersberger E (1992) Thermochim Acta 11(1):167
29. Echevskii GV, Kalinina NG, Anufrienko VF, Poluboyarov VA (1987) React Kinet Catal Lett 33(8):305
30. Zhu J, Uhl F, Morgan AB, Wilkie CA (2001) Chem Mater 13:4649–4654
31. Gilman GW, Jackson CL, Morgan AB, Harris RH, Manias E, Giannelis EP, Wuthenow M, Hilton D, Phillips S (2000) Chem Mater 12:1866
32. Kashiwagi T, Harris RH Jr, Zhang X, Briber RM, Cipriano BH, Raghavan SR, Awad WH, Shields JR (2004) Polymer 45:881